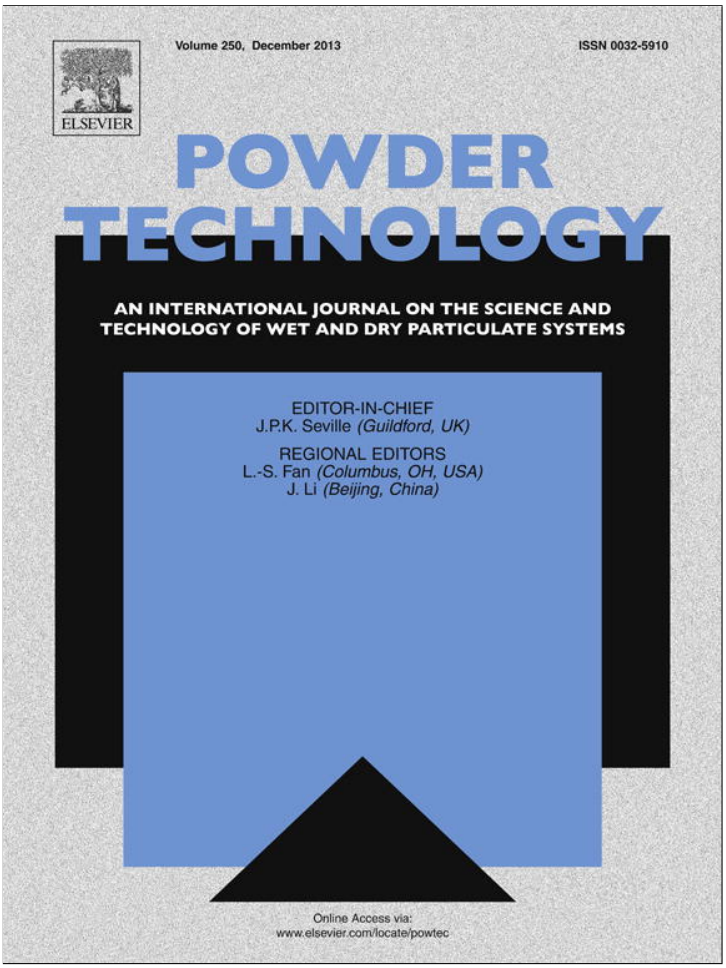

Powder Technology 250 (2013) 40–45

Contents lists available at ScienceDirect

Powder Technology

journal homepage: www.elsevier.com/locate/powtec

Three-dimensional SnO_2 microstructures assembled by porous nanosheets and their superior performance for gas sensing

Jing Guo, Jun Zhang *, Dianxing Ju, Hongyan Xu, Bingqiang Cao *

Key Laboratory of Inorganic Functional Materials in Universities of Shandong, School of Materials Science and Engineering, University of Jinan, Jiwei Road 106, Jinan 250022, China

ARTICLE INFO

Article history:
Received 12 June 2013
Received in revised form 26 August 2013
Accepted 1 October 2013
Available online 9 October 2013

Keywords:
SnO_2 nanosheets
Microstructure
Gas sensor
Sensitivity
Long-term stability

ABSTRACT

Nowadays, developing a simple, efficient, and low-cost route for synthesizing three-dimensional (3D) micro/nanostructures has become the research focus of nanomaterials. In this work, 3D SnO_2 microstructures assembled by nanosheets were prepared by hydrothermal synthesis combined with subsequent heat treatment. The morphology and crystal structure of the SnO_2 were characterized by X-ray diffraction, field emission scanning electron microscope, transmission electron microscope and N_2 adsorption–desorption isotherms. The as-prepared tin oxide samples show 3D hierarchical structures assembled with two-dimensional nanosheets. After sintering at 500 °C, the sample has better crystallinity of SnO_2 with a larger specific surface area of 62.5 m^2/g than that (24.1 m^2/g) of commercial SnO_2 materials. The 3D SnO_2 microstructures have been studied for ethanol gas sensing, showing good response–recovery performance, high sensitivity and excellent long-term stability and repeatability even after 4 months. The results demonstrate that 3D SnO_2 microstructures are promising for application as a gas sensor material.

1. Introduction

Gas sensors have attracted much attention by its application in air quality monitor and control, toxic or flammable gases detection, and medical diagnosis [1,2]. Great efforts have been made to improve the properties of gas sensors, including the sensitivity, selectivity, stability, and response–recovery speed (4S) [3], through many ways like tuning the size and morphology of working materials, preparing novel composite materials [4–8], and loading noble metal elements [7–11]. Special attention has been paid to the design of three-dimensional (3D) complex micro/nanostructures or hierarchical structures for optimum detection. Metal oxides with a 3D porous structure usually exhibit enhanced sensing performances in comparison with the similar bulk materials, due to the large active surface area and enhanced gas diffusion in sensing materials [12–15].

Many oxide semiconductors, such as ZnO [16,17], SnO_2 [18–21], WO_3 [22], Fe_2O_3 [23], and CuO [24], have been widely studied due to their good potential for gas sensor. Among the above semiconductors, SnO_2 has received particular interest for gas sensing because of its better sensing ability to a variety of gases and improved performance [25] including high sensitivity and stability, which is usually better than other metal oxides. Due to the influence of size and morphology on the material properties, SnO_2 with various nanostructures have been synthesized including nanoparticles [26,27], nanowires [28,29], nanorods [1,30], nanowhiskers [31], nanotubes [32], nanobelts [33,34], nanosheets [35,36], nanoflowers [37,38], and hollow spheres [2]. Although the low dimensional materials such as 0D nanoparticles and 1D nanorods usually have a higher surface area than the 3D microstructures, they suffer from poor stability due to sintering when used for resistive gas sensor working at elevated operating temperatures. In contrast, the 3D microstructures with a robust architecture could provide enhanced stability, because the sensing layer could well preserve the 3D structure against long-term working. In addition, it is well known that the sensing mechanism of SnO_2 is surface-controlled [5], the 3D microstructures also provide large inner voids, facile transport pathways or channels and high accessibility of materials surface to gas molecules, which are more conducive to the diffusion of target gas in the sensing layers [16,18].

In this paper, we mainly concentrate on synthesizing 3D SnO_2 microstructures through an environment friendly hydrothermal method and their sensor application. The 3D SnO_2 microstructures are assembled with 2D nanosheet blocks, which form large space among the nanosheets. Furthermore, the nanosheets also have a porous feature that could further increase the active surface area of the materials and provides facile pathways for the target gas. These features significantly enhance the sensor performances of the 3D SnO_2 microstructures.

2. Experimental

2.1. Synthesis of 3D SnO_2 microstructures

Stannous chloride dehydrate ($SnCl_2 2H_2O$), sodium hydroxide (NaOH), hexadecyltrimethylammonium bromide (CTAB), and ethanol, were all of analytical grades and were used as received from Sinopharm, China, without further purification. Commercially available

* Corresponding authors. Tel.: +86 531 8973 6292; fax: +86 531 8276 4453.
E-mail addresses: mse_zhangj@ujn.edu.cn (J. Zhang), mse_caobq@ujn.edu.cn (B. Cao).

0032-5910/$ – see front matter © 2013 Elsevier B.V. All rights reserved.
http://dx.doi.org/10.1016/j.powtec.2013.10.002

SnO_2 particles were also obtained from this company for the gas sensing test for comparison. SnO_2 microstructures were prepared via a hydrothermal process. In a typical synthesis, 0.46 g of $SnCl_2 2H_2O$ was introduced into 20 mL deionized water under stirring. Then 20 mL of aqueous solution containing 0.33 g NaOH and 0.74 g CTAB were added and the mixture was stirred for another 40 min. Afterwards, the mixture was transferred into a Teflon-lined stainless steel autoclave of 50 mL capacity. The autoclave was sealed and kept in an electrical oven at a constant temperature of 120 °C for 12, 24 and 48 h, respectively. After reaction, the autoclave was water-cooled rapidly. The yellow precipitate was collected by centrifugation and washed several times with ethanol and deionized water successively. Finally, the samples were dried at 80 °C and further annealed in a muffle furnace at 500 °C for 2 h for further characterizations and device fabrication.

2.2. Sample characterizations

Phase and structure identification was measured with power X-ray diffraction (XRD) using a Bruker diffractrometer (D8-Advance) with Cu Kα radiation of 1.5418 Å. The morphologies of the prepared SnO_2

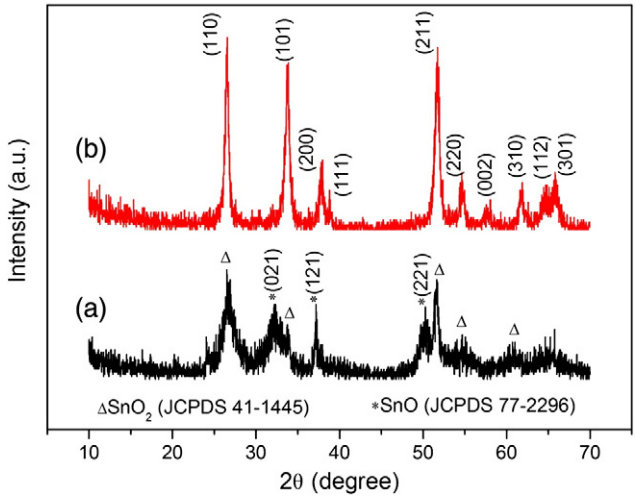

Fig. 1. XRD patterns of (a) as-prepared 24 h SnO_2 microstructures and (b) heat-treated products.

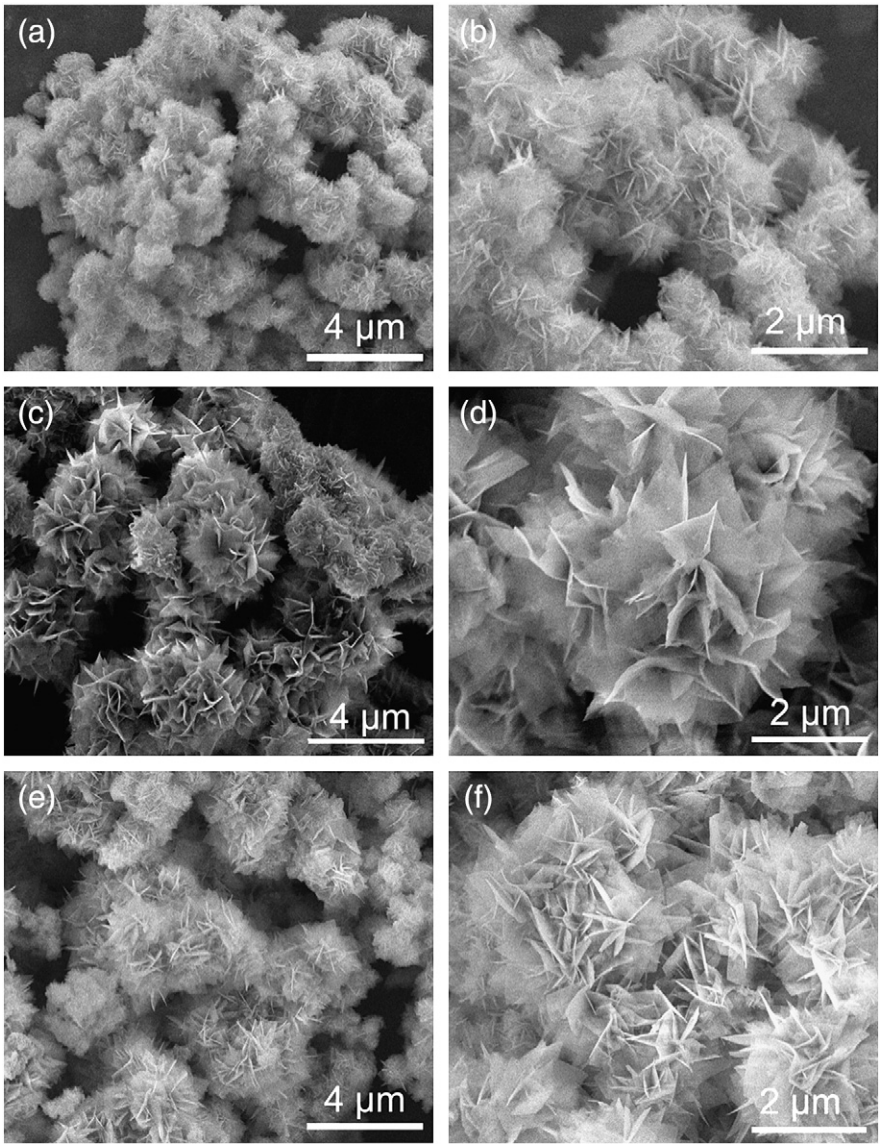

Fig. 2. SEM images of SnO_2 nanosheets with different reaction time: (a, b), (c, d) and (e, f) represent samples prepared at different reaction time of 12, 24, 48 h, respectively.

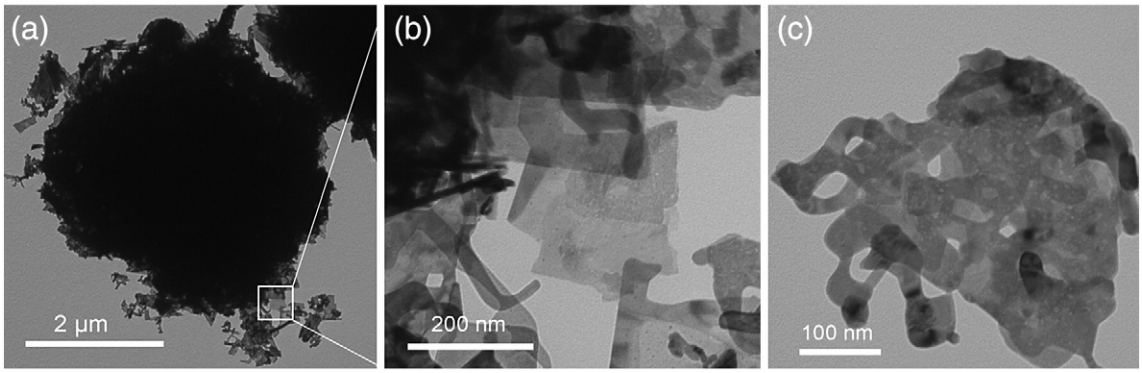

Fig. 3. TEM images of (a) 3D SnO_2 microstructure, and (b, c) SnO_2 nanosheets.

microstructures were observed with a scanning electron microscope (SEM, Quanta FEG 250, 30 kV) and transmission electron microscope (TEM, JEM-1011, 100 kV), respectively. The Brunauer–Emmett–Teller (BET) specific surface area was measured with a N_2 adsorption–desorption analyzer (3 W-BK, Beijing).

2.3. Sensor fabrication and measurements

The gas sensors were fabricated as described in the literature [3]. Briefly, a small amount of SnO_2 sample was ground in an agate mortar with several drops of deionized water. The slurry was slightly coated onto an alumina tube to form a thin film. The alumina tube has a diameter of 1 mm and length of 4 mm with a pair of Au electrodes and four Pt wires on both ends. A Ni–Cr alloy coil through the tube worked as a heater to control the operating temperature by tuning the heating voltage. Gas sensing tests were performed by a WS-60A gas sensing measurement system (HanWei Electronics, China) at a relative humidity (RH) of 25%. WS-60A is a static system using atmospheric air as the reference and dilute gas. Target gas with calculated amount is introduced into the test chamber by a syringe. Two electric fans installed in the chamber are used to make test gas homogeneous. After test, the chamber was removed for sensor recovery. The sensor response is defined as the ratio $S = R_a/R_g$, where R_a and R_g are the resistance of the sensor in air and in target gas, respectively.

3. Results and discussion

The XRD patterns of the as-prepared and annealed SnO_2 microstructures with reaction time of 24 h are shown in Fig. 1. The XRD pattern of the as-prepared sample shows a mixture phase containing both SnO (JCPDS No. 77–2296) and SnO_2 (JCPDS No. 41–1445) of poor crystallization as the diffraction peaks are rather weak and broad. After annealing at 500 °C for 2 h, the sample is of higher crystallinity, as observed in Fig. 1(b) and all the diffraction peaks can be well indexed to the tetragonal rutile structure of SnO_2. It also indicates the SnO has completely transformed into SnO_2 due to oxidation after the annealing process. The crystallite size of the 3D SnO_2 materials is calculated to be 20.5 nm with the Scherrer equation based on (110) peak.

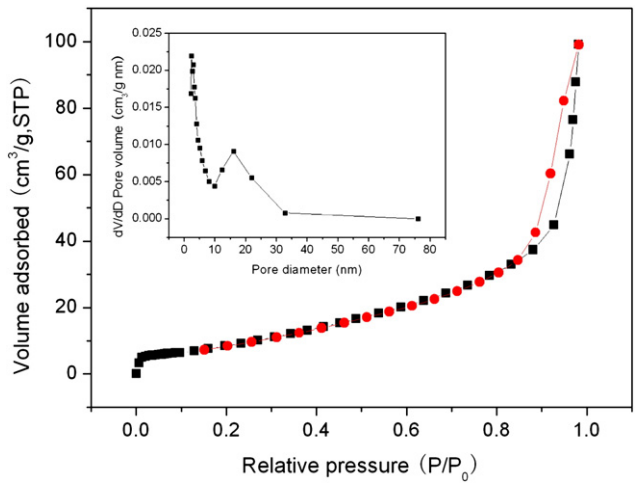

Fig. 4. Nitrogen adsorption–desorption isotherm and pore size distribution curve (inset) of the 24 h nanostructures.

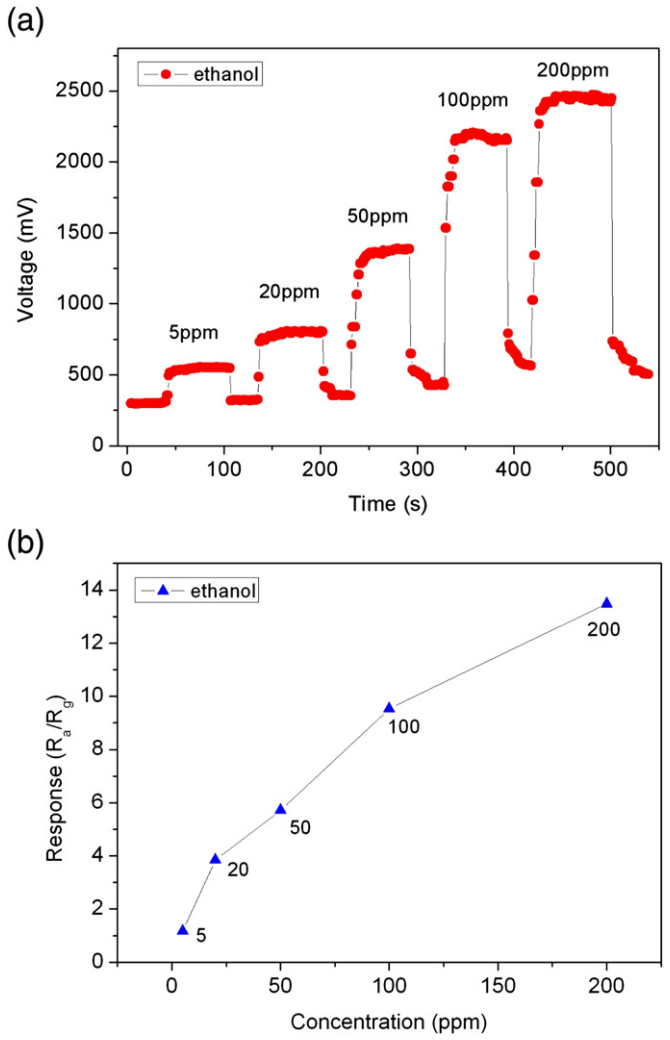

Fig. 5. Response–recovery curve (a) and response of 3D SnO_2 microstructures at 300 °C to different concentration of ethanol (b).

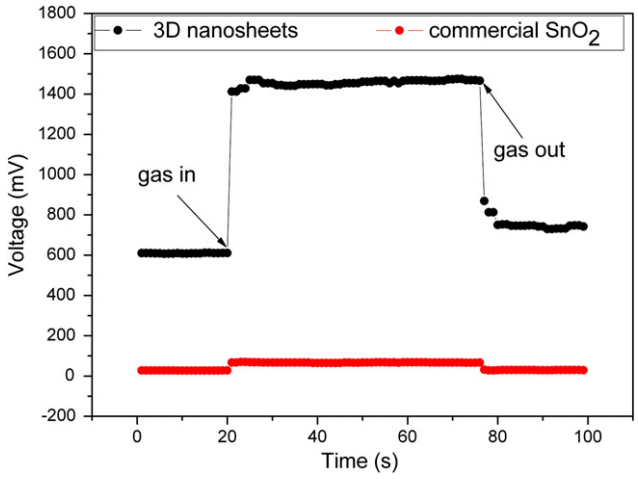

Fig. 6. The dynamic response–recovery curve to 50 ppm ethanol of 3D microstructures and commercial SnO_2.

The effect of reaction time on the morphology and size of the SnO_2 microstructures was investigated by varying the reaction time as 12, 24 and 48 h. Fig. 2 shows the SnO_2 morphologies grown under different reaction time that all exhibit 3D hierarchical microstructures composed of 2D SnO_2 nanoplates. Based on this, we proposed a growth mechanism of the 3D SnO_2 microstructures. At the initial stage of the reaction, fine SnO_2 clusters were generated and nucleated together. The primary small crystallites aggregated in the form of nanosheets in order to lower the surface energy [39,40], which finally self-assembled into 3D microstructures. With the increase of reaction time, the sheets grew larger, as shown in Fig. 2(a, b) and (c, d). However, if the reaction time is further extended to 48 h, the morphology of the nanosheets shows no obvious change.

The 3D SnO_2 microstructures were further characterized with TEM. Fig. 3 displays typical TEM images of SnO_2 microstructures grown with 24 h. From Fig. 3(a, b), it is observed that the 3D structure is assembled by many nanoplates with a size of hundreds of nanometers. Fig. 3(c) shows a representative individual SnO_2 nanoplate, revealing that there exist many pores in the SnO_2 nanoplate. The formation of these pores might be caused by the sintering and crystallization of SnO_2 in the calcination process at elevated temperature [41]. As can be seen in the XRD pattern, the product after calcination has much

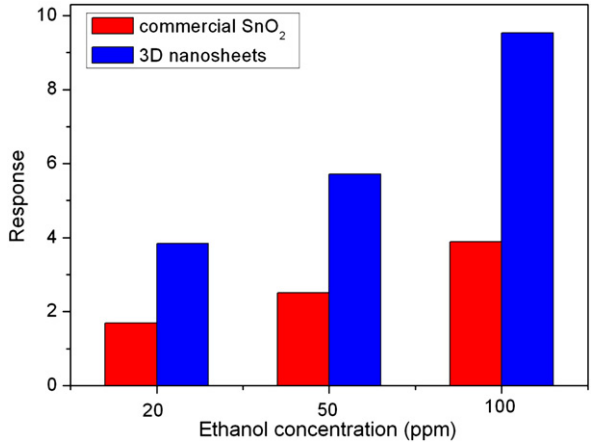

Fig. 7. The response of commercial SnO_2 materials and 3D microstructures to different concentrations of ethanol.

Table 1
Comparisons of response towards ethanol of gas sensors assembled with various SnO_2 nanostructures.

SnO_2 sensor	Nanowire [4]	Nanoflower [39]	Nanotube [42]	Thin film [43]	Our work
Ethanol (ppm)	100	100	100	200	100
Response	<2	7	<8	4.8	10

higher crystallinity. Clearly, such porous feature could further increase the 3D microstructure surface area, which is advantageous for the surface sensing applications [26].

The BET specific surface area of the 3D SnO_2 microstructures was measured by N_2 adsorption–desorption isotherms. Fig. 4 shows the nitrogen adsorption–desorption isotherm and pore size distribution curve of the sample shown in Fig. 3. The hysteresis loop locates at the range of 0.8–0.98 in the isotherm. The pore size distribution curve reveals that the SnO_2 has a porous structure and the pore size is in the range of 2–50 nm. The BET specific surface area is determined to be 62.5 m^2/g.

Inspired by their unique 3D microstructure, we examined the gas sensing properties by fabricating gas sensors using the 3D SnO_2 powders as working medium. The gas sensing experiments were carried out at an operating temperature of 300 °C. Fig. 5(a) shows the dynamic response–recovery curve of nanosheet sensor to ethanol of different concentrations. It is obvious that the response amplitude increases with ethanol concentration increasing. The sensor shows high response to ethanol even at a low concentration of 5 ppm. The sensor responses to various ethanol concentrations were plotted in Fig. 5(b). With the increase of ethanol concentration, more target gas molecules participate in the surface sensing reaction resulting in the enhancement of sensor response. In Fig. 5(b), it shows that the sensor is capable to discriminate different ethanol concentrations in the range of 5–200 ppm.

In order to prove the effect of the 3D microstructure on sensor properties, we also measured the gas sensing property of commercial SnO_2 particles for comparison. Fig. 6 shows the dynamic response–recovery curves of the two sensors to 50 ppm ethanol. It is clear that the response amplitude of the 3D SnO_2 is much higher, while the commercial SnO_2 powders only show very small response. Fig. 7 compares the response values of the commercial SnO_2 powders with 3D SnO_2 microstructures to ethanol of different concentrations. Both sensors exhibit increasing response with the growth of ethanol concentration. However, the response of 3D SnO_2 nanostructures is nearly twice higher than that of commercial SnO_2 materials. Moreover, compared with the sensors based on other SnO_2 nanostructures reported in literature [4,39,42,43], our 3D SnO_2 microstructure manifests superior performances to 100 ppm ethanol in terms of higher response, as summarized in Table 1.

We suppose that the enhanced sensor response of SnO_2 should be ascribed to the unique 3D porous microstructure [44]. To prove this hypothesis, the structure of commercial SnO_2 materials is also observed by SEM. Fig. 8(a, b) displays the SEM images of commercial SnO_2 particles with different magnifications. Compared with the SEM images of 3D porous microstructure in Fig. 2, the commercial SnO_2 materials contain many particles of different size. Thus it is speculated that the sensor film made from the commercial SnO_2 particles should be denser than that from the 3D porous SnO_2 microstructures. Moreover, the single nanoplates with holes could also increase the surface area and accelerate the diffusion of gas within sensing film. According to our N_2 adsorption–desorption analysis, the commercial SnO_2 has a specific surface area of only 24.1 m^2/g, which is much smaller than that (62.5 m^2/g) of 3D SnO_2 microstructures. It is reasonable that the large specific surface area of the 3D SnO_2 leads to the enhanced sensing performance.

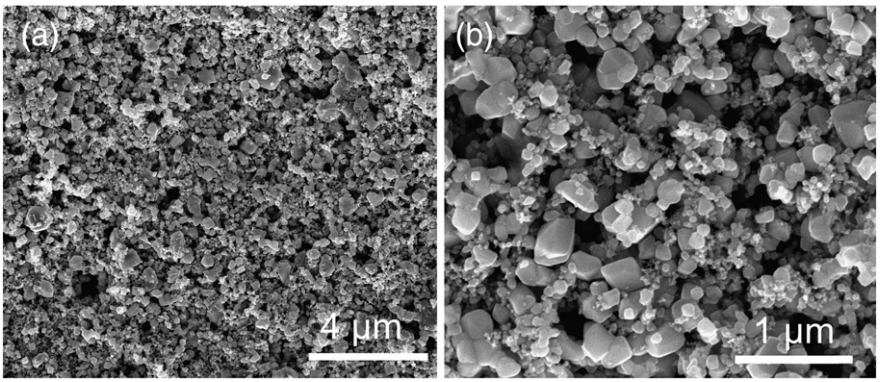

Fig. 8. SEM (a, b) with different magnifications of commercial SnO_2 particles.

The repeatability and long-term stability of the 3D SnO_2 sensor were investigated by measuring ethanol of 150 ppm with six cycles at operating temperature of 300 °C. As shown in Fig. 9, the sensor exhibits very fast response and recovery even after 4 months and has very excellent repeatability and stability. Such good feature of the 3D SnO_2 microstructures is very useful for fabricating gas sensor with long life from the point view of practical applications. Moreover, the selectivity of the 3D SnO_2 was also investigated by detecting different gases. As shown in Fig. 10, all the gas responses were tested at 300 °C with the same concentration of 50 ppm. It reveals that the 3D SnO_2 sensor manifests the highest response of 5.1 to ethanol, which is much higher than that to methanol (3.0) and acetone (2.1).

SnO_2 is a typical n-type semiconductor and it is also known as a surface-controlled type of sensor material. Generally, oxygen molecules in air are adsorbed on the surface of SnO_2. They capture electrons from the conduction band of metal oxides in the form of oxygen species like O_2^-, O^- and O^{-2}. An electron depletion layer is thus formed on the surface of SnO_2 [45,46] as shown in Fig. 11(a), which leads to the increase of resistance. When this process reaches to a balance, the sensor resistance is stable. Once reducing gas such as ethanol is introduced into the test chamber, it will be oxidized by the oxygen species (O_2^-, O^- and O^{-2}) immediately and then the electrons will be released back to the conduction band and decrease the electron depletion layer as shown in Fig. 11(b), which will decline the resistance of the sensor. When the ethanol gas is removed, oxygen molecules will be re-absorbed on the surface of SnO_2 to refresh the gas sensor [35]. In addition, it is expected that combining the 3D metal oxide microstructures with noble metal nanoparticles could further improve the sensor performance. Detailed work is underway in our lab.

4. Conclusions

In this work, we have synthesized 3D SnO_2 microstructures composed of 2D porous nanosheets by hydrothermal synthesis combined with subsequent heat treatment. The 3D structures together with the porous nanosheets endow the SnO_2 materials with large surface area and easy gas diffusion, which is very beneficial for gas sensing applications. Ethanol gas sensing tests demonstrate that the 3D SnO_2 microstructures show superior performance with respect to fast response, high repeatability, and long-term stability. The good sensing features indicate the present 3D SnO_2 microstructures are promising for gas sensors.

Acknowledgments

This work is supported by the Program for New Century Excellent Talents in University (NCET-11-1027) of MOE, China, and Shandong Provincial Science Foundation for Disguised Youth Scholars (JQ201214) and Excellent Young and Middle-aged Scientists (BS2012CL003). BC thanks the Taishan Scholar Professorship (TSHW20091007) and JZ thanks the Research Fund (XKY11111) for new Faculty both tenured at University of Jinan.

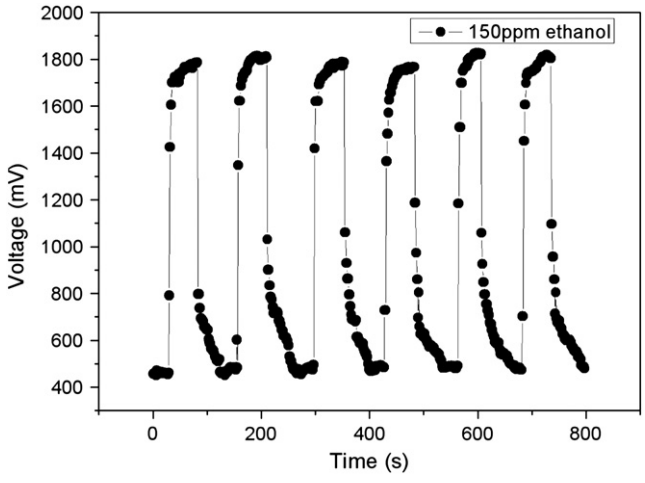

Fig. 9. Response–recovery curve of the 3D SnO_2 sensor to 150 ppm ethanol at 300 °C after 4 months.

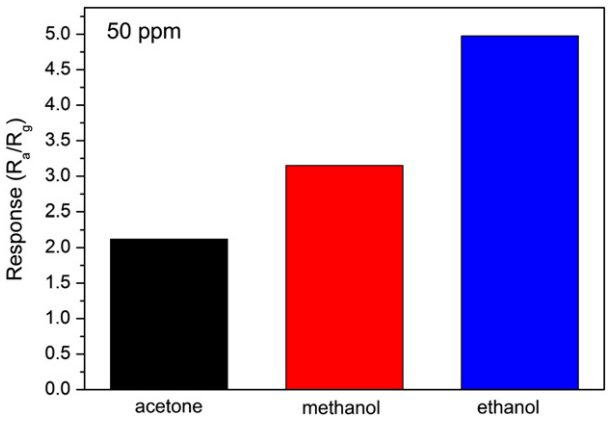

Fig. 10. Comparison of sensor responses to 50 ppm acetone, methanol and ethanol.

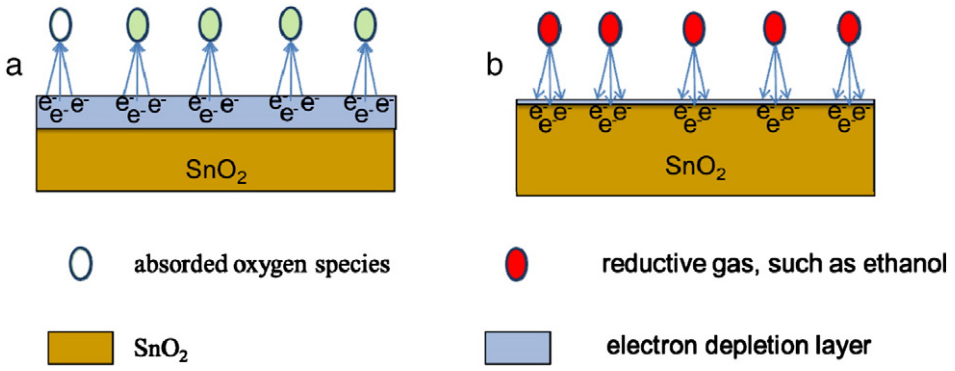

Fig. 11. Scheme for the gas sensing process of the nanosheets.

References

[1] V.V. Sysoev, B.K. Button, K. Wepsiec, S. Dmitriev, Toward the nanoscopic "Electronic Nose": hydrogen vs carbon monoxide discrimination with an array of individual metal oxide nano- and mesowire sensors, Nano Lett. 6 (2006) 1584–1588.

[2] F. Sun, W. Cai, Y. Li, L. Jia, F. Lu, Direct growth of mono- and multilayer nanostructured porous films on curved surfaces and their application as gas sensors, Adv. Mater. 17 (2005) 2872–2877.

[3] J. Zhang, S.R. Wang, Y.M. Wang, Y. Wang, B.L. Zhu, H.J. Xia, X.Z. Guo, S.M. Zhang, W.P. Huang, S.H. Wu, NO_2 sensing performance of SnO_2 hollow-sphere sensor, Sens. Actuators B 135 (2009) 610–617.

[4] N.D. Khoang, D.D. Trung, N.V. Duy, N.D. Hoa, N.V. Hieu, Design of SnO_2/ZnO hierarchical nanostructures for enhanced ethanol gas-sensing performance, Sens. Actuators B 174 (2012) 594–601.

[5] S. Hemmati, A.A. Firooz, A.A. Khodadadi, Y. Mortazavi, Nanostructured SnO_2-ZnO sensors: highly sensitive and selective to ethanol, Sens. Actuators B 160 (2011) 1298–1303.

[6] W.W. Guo, T.M. Liu, R. Sun, Y. Chen, W. Zeng, Z.C. Wang, Synthesis of unique ZnO/SnO_2 core–shell structural microspheres and their gas-sensing properties, Mater. Lett. 89 (2012) 5–8.

[7] A. Nakajima, A study of SnO_2-based gas sensors affected by addition of several metal oxides, J. Mater. Sci. Lett. 12 (1993) 1778–1780.

[8] X.H. Liu, J. Zhang, X.Z. Guo, S.R. Wang, S.H. Wu, Core-shell α-Fe_2O_3@SnO_2/Au hybrid structures and their enhanced gas sensing properties, RSC Advances 2 (2012) 1650–1655.

[9] A. Kolmakov, D.O. Klenov, Y. Lilach, S. Stemmer, M. Moskovits, Enhanced gas sensing by individual SnO_2 nanowires and nanobelts functionalized with Pd catalyst particles, Nano Lett. 5 (2005) 667–673.

[10] X.H. Liu, J. Zhang, X.Z. Guo, S.H. Wu, S.R. Wang, Enhanced sensor response of Ni-doped SnO_2 hollow spheres, Sens. Actuators B 152 (2011) 162–167.

[11] X.H. Liu, J. Zhang, L.W. Wang, T.L. Yang, X.Z. Guo, S.H. Wu, S.R. Wang, 3D hierarchically porous ZnO structures and their functionalization by Au nanoparticles for gas sensors, J. Mater. Chem. 21 (2011) 349–356.

[12] M.C. Jeong, B.Y. Oh, O.H. Nam, T. Kim, J.M. Myoung, Three-dimensional ZnO hybrid nanostructures for oxygen sensing application, Nanotechnology 17 (2006) 526–530.

[13] M. Tiemann, Porous metal oxides as gas sensors, Chem. Eur. J. 13 (2007) 8376–8388.

[14] Z.R. Li, X.L. Li, X.X. Zhang, Y.T. Qian, Hydrothermal synthesis and characterization of novel flower-like zinc-doped SnO_2 nanocrystals, J. Cryst. Growth 291 (2006) 258–261.

[15] C.H. Wang, X.F. Chu, M.M. Wu, Highly sensitive gas sensors based on hollow SnO_2 spheres prepared by carbon sphere template method, Sens. Actuators B 120 (2007) 508–513.

[16] J. Zhang, S.R. Wang, M.J. Xu, Y. Wang, B.L. Zhu, S.M. Zhang, W.P. Huang, S.H. Wu, Hierarchically porous ZnO architectures for gas sensor application, Cryst. Growth Des. 9 (2009) 3532–3537.

[17] P. Rai, S. Raj, K.J. Ko, K.K. Park, Y.T. Yu, Synthesis of flower-like ZnO microstructures for gas sensor applications, Sens. Actuators B 178 (2013) 107–112.

[18] L.L. Wang, Z. Lou, T. Zhang, H.T. Fan, X.J. Xu, Facile synthesis of hierarchical SnO_2 semiconductor microspheres for gas sensor application, Sens. Actuators B 155 (2011) 285–289.

[19] Y.Q. Guo, Y. Li, R.Q. Tan, W.J. Song, Synthesis of SnO_2 hollow microspheres with core-shell structures through a facile template-free hydrothermal method, Mater. Sci. Eng. B (2010) 20–24.

[20] M.M. Titirici, M. Antonietti, A. Thomas, A generalized synthesis of metal oxide hollow spheres using a hydrothermal approach, Chem. Mater. 18 (2006) 3808–3812.

[21] M. Wang, Y.F. Gao, L. Dai, C.X. Cao, X.H. Guo, Influence of surfactants on the morphology of SnO_2 nanocrystals prepared via a hydrothermal method, J. Solid State Chem. 189 (2012) 49–56.

[22] X.H. Liu, J. Zhang, T.L. Yang, X.Z. Guo, S.H. Wu, S.R. Wang, Synthesis of Pt nanoparticles functionalized WO_3 nanorods and their gas sensing properties, Sens. Actuators B Chem. 156 (2011) 918–923.

[23] Y. Liu, W. Zhu, O.K. Tan, Y. Shen, Structural and gas sensing properties of ultrafine Fe_2O_3 prepared by plasma enhanced chemical vapor deposition, Mater. Sci. Eng. B 47 (1997) 171–176.

[24] Y.M. Li, J. Liang, Z.L. Tao, Jun Chen, CuO particles and plates: synthesis and gas-sensor application, Mater. Res. Bull. 43 (2008) 2380–2385.

[25] David E. Williams, Semiconducting oxides as gas-sensitive resistors, Sens. Actuators B 57 (1999) 1–16.

[26] L.J. Xi, D. Qian, X.C. Tang, C.J. Chen, High surface area SnO_2 nanoparticles: synthesis and gas sensing properties, Mater. Chem. Phys. 108 (2008) 232–236.

[27] H.C. Chiu, C.S. Yeh, Hydrothermal synthesis of SnO_2 nanoparticles and their gas-sensing of alcohol, J. Phys. Chem. C 111 (2007) 7256–7259.

[28] Q. Kuang, C.S. Lao, Z.L. Wang, Z.X. Xie, L.S. Zhang, High-sensitivity humidity sensor based on a single SnO_2 nanowire, J. Am. Chem. Soc. 129 (2007) 6070–6071.

[29] D.D. Trung, N.V. Toan, P.V. Tong, N.V. Duy, N.D. Hoa, N.V. Hieu, Synthesis of single-crystal SnO_2 nanowires for NOx gas sensors application, Ceram. Int. 38 (2012) 6557–6563.

[30] C.X. Guo, M.H. Cao, C.W. Hu, A novel and low-temperature hydrothermal synthesis of SnO_2 nanorods, Inorg. Chem. Commun. 7 (2004) 929–931.

[31] Z. Ying, Q. Wan, Z.T. Song, S.L. Feng, SnO_2 nanowhiskers and their ethanol sensing characteristics, Nanotechnology 15 (2004) 1682–1684.

[32] Z.J. Li, H.Y. Wang, P. Liu, B. Zhao, Y.F. Zhang, Synthesis and field-emission of aligned SnO_2 nanotubes arrays, Appl. Surf. Sci. 255 (2009) 4470–4473.

[33] M.S. Arnold, P. Avouris, Z.W. Pan, Z.L. Wang, Field-effect transistors Based on single semiconducting oxide nanobelts, J. Phys. Chem. B 107 (2003) 659–663.

[34] E. Comini, G. Faglia, G. Sberveglieri, Stable and highly sensitive gas sensors based on semiconducting oxide nanobelts, Appl. Phys. Lett. 81 (2002) 1869–1871.

[35] Z. Lou, L.L. Wang, R. Wang, T. Fei, T. Zhang, Synthesis and ethanol sensing properties of SnO_2 nanosheets via a simple hydrothermal route, Solid-State Electron. 76 (2012) 91–94.

[36] H.D. Liu, J.M. Huang, X.L. Li, J. Liu, Y.X. Zhang, Green synthesis of SnO_2 nanosheets and their electrochemical properties, Ceram. Int. 39 (2013) 3413–3415.

[37] Z.D. Lin, W.L. Song, H.M. Yang, Highly sensitive gas sensor based on coral-like SnO_2 prepared with hydrothermal treatment, Sens. Actuators B 173 (2012) 22–27.

[38] L.M.J.W. Deng, X.M. Yin, M. Zhang, Q.H. Li, E.D. Zhang, Z. Xu, L.B. Chen, T.H. Wang, Ultrasensitive ethanol sensor based on 3D aloe-like SnO_2, Sens. Actuators B 166–167 (2012) 7–11.

[39] L.W. Wang, S.R. Wang, Y.S. Wang, H.X. Zhang, Y.F. Kang, W.P. Huang, Synthesis of hierarchical SnO_2 nanostructures assembled with nanosheets and their improved gas sensing properties, Sens. Actuators B 188 (2013) 85–93.

[40] H.B. Wu, J.S. Chen, X.W. (David) Lou, H.H. Hng, Synthesis of SnO_2 hierarchical structures assembled from nanosheets and their lithium storage properties, J. Phys. Chem. C 115 (2011) 24605–24610.

[41] B.X. Li, Y.F. Wang, Hierarchically assembled porous ZnO microstructures and applications in a gas sensor, Superlattice. Microst. 49 (2011) 433–440.

[42] G.X. Wang, J.S. Park, M.S. Park, X.L. Gou, Synthesis and high gas sensitivity of tin oxide nanotubes, Sens. Actuators B 131 (2008) 313–317.

[43] K.W. Kim, P.S. Cho, S.J. Kim, J.H. Lee, C.Y. Kang, J.S. Kim, S.J. Yoon, The selective detection of C_2H_5OH using SnO_2-ZnO thin film gas sensors prepared by combinatorial solution deposition, Sens. Actuators B 123 (2007) 318–324.

[44] W.W. Guo, T.M. Liu, J.X. Wang, W.J. Yu, R. Sun, Y. Chen, S. Hussain, X.H. Peng, Z.C. Wang, Hierarchical ZnO porous microspheres and their gas-sensing properties, Ceram. Int. 39 (2013) 5919–5924.

[45] S.R. Morrison, Selectivity in semiconductor gas sensors, Sens. Actuators B 12 (1987) 425–440.

[46] J. Zhang, X.H. Liu, S.H. Wu, B.Q. Cao, S.H. Zheng, One-pot synthesis of Au-supported ZnO nanoplates with enhanced gas sensor performance, Sens. Actuators B 169 (2012) 61–66.